

Objective mapping of observed sub-surface mesoscale cold core eddy in the Bay of Bengal by stochastic inverse technique with tomographically simulated travel times

T.V. Ramana Murty*, M.M. Malleswara Rao, Y. Sadhuram, B. Sridevi, K. Maneesha

S. Sujith Kumar, P.L.Prasanna and K.S.R. Murthy

National Institute of Oceanography, Regional Center (CSIR), 176, Lawson's Bay Colony, Visakhapatnam –5300 17.

*[E-mail : tvrmurty@nio.org]

Received 07 December 2010; revised 11 January 2011

Present study consists the acoustic characteristics of a sub-surface cold core eddy observed (below the mixed layer between depths of 50 and 300m, with a diameter of about 200 km having temperature drop of 5°C at the center) in the Bay of Bengal during south-west monsoon season and explore possibility to reconstruct the acoustic profile of the eddy by Stochastic Inverse Technique. A simulation experiment on forward and inverse problems for observed sound velocity perturbation field has been attempted for a range of 650 km (in the vertical slice) keeping the single source-receiver configuration (at the channel axis depth) in the SOFAR channel, under peculiar characteristics viz, depth-limited environment and weak gradient waters of the Bay of Bengal. For the formulation of the Stochastic Inverse, both vertical and horizontal structure of the ocean has been modeled using empirical orthogonal modes. Present Ocean Acoustic Tomography's (OAT's) simulation experiment results reveal that one can objectively map/monitor even the small mesoscale sub-surface eddies by stochastic inverse technique keeping single source and receiver in the SOFAR channel separated probably by larger distances also under such depth-limited environment of the Bay of Bengal.

[Keywords: Tomography, cold core eddy, Bay of Bengal, Forward problem, Inverse problem, EOF, Stochastic Inverse, SOFAR channel, acoustic modeling].

Introduction

Understanding oceanic weather and its effect on the general ocean circulation is now the fundamental problem of the ocean dynamics and is a prerequisite to the formation of coupled ocean – atmospheric models necessary for weather prediction and climate trend analysis¹. As these eddies transport and disperse chemicals, dissolved substances, particulate matter, nutrients, heat and small organisms in the sea²⁻³, observational methods/tools covering synoptic scales are essential. Unlike atmospheric weather the mesoscale variability of ocean is difficult to observe. Eddies are always found in all the oceans and in all the seasons with different spatial, time scales and energy levels⁴⁻⁵. The scales of mesoscale eddy are: a few hundred kilometers in the tropics, of the order of a hundred kilometers in the subtropics, and a few tens of kilometers in the high latitudes⁶. Meso-scale eddies are known to exist in the Bay of Bengal from 1957 onwards were reported by several authors⁷⁻¹². Eddies in the Bay of Bengal are influenced by the unique

seasonal reversing monsoons and transient cyclonic storms¹³.

In recent past, a cold core sub-surface eddy (below 50 m depth from surface) having diameter 200 km with Available Potential Energy (APE) of $1.31 \times 10^2 \text{ J/m}^3$ was reported^{10,14} in the northwestern Bay of Bengal, based on the CTD data collected during southwest monsoon season. The estimated energy content of the mesoscale eddy field may be many times to that of the general ocean circulation¹⁵. Even though no biological observations were made, it was obvious that surface water in that region near the center of observed cyclonic cold core eddy quite productive¹⁶⁻¹⁹. Similarly, such cyclonic eddies also may play a significant role in the interaction with the atmosphere, by raising the thermocline locally and enabling surface temperature anomalies more readily by downward mixing¹³.

Satellite remote sensing technique is one of the aspects of monitoring such mesoscale variability². But satellite receivers using infrared radiance imagery

have shown some promise for detecting sea surface variations but mesoscale variability prevails in the deeper ocean is not at all possible to detect. This is true for highly stratified nature of waters of the Bay of Bengal due to fresh water discharge²⁰. Munk and Wunsch²¹ have suggested an alternative method called Ocean Acoustic Tomography (OAT). Tomography is a technique for observing the ocean and this is still relatively a new technique and a feasible experiment was conducted²² in 1981. This technique is analogous to the medical procedure called Computer Aided Tomography (CAT), which yields a two dimensional display of the anatomy of the part of the human body under investigation²³. OAT is a scheme to infer sound velocity or current velocity fields of the intervening ocean from the travel time of sound, which is the function of sound speed and current velocity. It has special advantage that, one can get the snapshots of small scale to large scale phenomena in the ocean, which is so difficult to fetch by conventional shipboard and mooring techniques. The velocity of sound in the ocean is as fast as 1.5 km/sec which permits the reconstruction of synoptic fields of data, which is equivalent to all that of one-point measurement stations, while N tomography stations produce the data number of ${}_N C_2$. With increasing number of the stations, the spatial resolution for the acoustic tomography becomes much better when compared with the conventional method. In OAT, path averaged data along the ray is used. Another advantage of the acoustic tomography is that it is one of the remote sensing techniques to explore ocean interior, where the direct observation is difficult due to ship traffic, fishing grounds, military training areas, etc, that become targets to be measured continuously by the tomography stations arrayed at the periphery of the observational region²⁴.

Materials and Methods

The OAT technique essentially attempts to estimate the state of the ocean at any given time using the travel time measurements of sound pulses between sound sources and receivers distributed at suitable locations in the SOFAR channel of the ocean. In this technique, we assume a reference ocean stratified in the vertical direction, and trace the sound ray paths from a source to a receiver (eigenrays). For this purpose, the climatologically mean state of the ocean could be used as the reference state. Tracing of the sound ray paths and estimation of sound pulse travel

time and its intensity at the receiver end, is referred to as the "Forward Problem".

The travel times for different ray paths measured in a real ocean will differ from the computed travel times for the reference ocean. This difference will be due to the perturbations in the prevailing thermal structure and the consequent perturbations in the sound velocity profile of the real ocean over that of the reference ocean. From the differences between the measured and the computed travel times and with information on environmental noise (if available), an estimate of the sound speed perturbation in the ocean along the ray paths may be obtained. The procedure adopted for the optimal estimation of the sound velocity perturbation from the travel time information is called the "Inverse Problem". The least square method, damped least square method and Gause-Markov method are introduced as suitable inversion techniques for the ocean acoustic tomography^{22,24}. The Gause-Markov method²⁵ has been used as the familiar technique. However, in the absence of statistical information, the least squares method may be an alternative. When the least squares method has problems related to smaller eigenvalues for coefficient matrix (data kernel), it is to be replaced by the damped least squares method^{26,27,24}. The inverse problem forms an important first step in the interpretation of the travel time data, collected by tomographic experiments, which would be ultimately used for the description of the ocean flow field.

In the recent past, a cold core, sub-surface eddy centered at 17° 40'N and 85°19'E in the northwestern Bay of Bengal was reported¹⁰ based on the Conductivity, Temperature, Depth (CTD) data collected at 42 stations onboard ORV Sagar Kanya during 21-29 July 1984. The physical interpretation of hydrographic data and triggering mechanism for generation of identified sub-surface cold core eddy are well described earlier¹⁰. Use of acoustics to monitor the interior of oceans using OAT's principle²⁸ explores possible means to reconstruct the acoustic profile of eddy (through application of generalized inverse technique) using simulated travel time perturbations under range independent environment.

Prasanna Kumar *et.al.*,²⁸ simulated tomographic inversion of a cold core eddy in the Bay of Bengal, under range-independent nature applying deterministic generalized inverse approach. The profile is depth limited with the effective acoustic wave guide situated much below the surface evidenced by the variation in

the conjugate depth (depth below the sea surface at which the sound velocity equals the near bottom value). The traced rays under range-independent environment were unable to scan the top layer (i.e., above the conjugate depth) and therefore its inverse solution gives layer-wise sound velocity perturbation in the average manner, as such unable to reconstruct eddy as it is in the objective manner. Since real ocean is of range-dependent nature, the same data of all eddy profiles used in the above paper revisited in the present OAT's simulation study to explore possible means to reconstruct the eddy, which is above the conjugate depth. And also, deterministic inverse procedure doesn't permit a continuous representation of unknown field, so we demonstrate in this paper how the adoption stochastic inverse technique²² works for the objective mapping. In the present OAT's acoustic simulation experiment, we have demonstrated that the single source and receiver (kept at the channel axis) in the SOFAR channel separated by distance of 650 km has been used to infer the distance to a mesoscale disturbance due to sub-surface cold core eddy under depth-limited nature of tropical environment. Finally we show, how OAT principle and use of stochastic inverse technique works to resolve cold core eddy due to few trapped acoustic rays above the conjugate depth.

Similar OAT simulation experiment, but with excess-depth environment, has been conducted elsewhere¹ from a single source to receiver separated by 1000 km. The following sections are included with required mathematics for OAT forward and inverse problems, details of data preparation needed for stochastic inverse framework and finally interpretation of the simulated results.

Forward problem

Sound waves, which propagate from the source to receiver, are influenced by the sound velocity $C(x, z)$ and current velocity $u(x, z)$ in the intervening water (Fig. 1). This is called the forward problem and the detailed properties of received signals can be calculated by solving the sound wave equation with the given values of C and u ⁴². Understanding the forward problem is so important to solve optimally, the inverse problem because received acoustic signals are to be identified for making the accurate and successful inversion. For the OAT studies, the forward problem is solved by the computer simulation in which *a priori* sound velocity data obtained in the observation region are used. The received signals can be identified by comparing the simulated (predicted) results with observed ones (experimental data).

In the OAT studies the observable data are travel times and intensities of received signals. While the later are out of scope in this study the former used in present inverse problem. Early and late arrival rays take different ray paths and thus have different sound and current velocity fields²⁴.

The travel times of sound between two acoustic transceivers along the reciprocal ray paths can be formulated as (in 2-D form)

$$T^{\pm} = \oint_{\Gamma^{\pm}} \frac{ds}{C(x, z) + u(x, z) \cdot n} \quad \dots (1)$$

where \pm represents the positive/negative direction from one transceiver to another, n the unit vector tangent to the ray path and s the arc length measured along the ray path. Γ^{\pm} are the positive and negative paths refracted by $C(x, z)$ and $u(x, z) \cdot n$. The ray paths

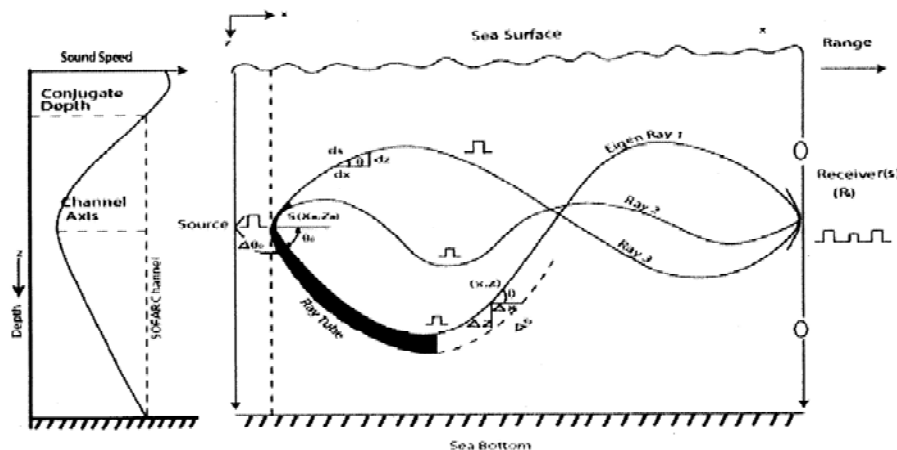


Fig. 1—Schematic presentation of acoustic rays from source to receiver

are generally not coincident for two ways in the reciprocal transmission, but we can approximate $\Gamma^+ \approx \Gamma^- \equiv \Gamma_0$ when $u \cdot n/C \ll 1$. The mean travel time perturbation δT and the differential travel time ΔT are expressed by

$$\delta T = \frac{1}{2}(T^+ + T^-) - T_0 \approx -\oint_{\Gamma_0} \frac{\delta C(x, z)}{C_0(z)^2} ds \quad \dots (2)$$

$$\Delta T = \frac{1}{2}(T^+ - T^-) \approx -\oint_{\Gamma_0} \frac{u(x, z) \cdot n}{C_0(z)^2} ds \quad \dots (3)$$

where T_0 the travel time along the ray path is Γ_0 is associated with a reference sound speed $C_0(z)$ and $\delta C(x, z) (= C(x, z) - C_0(z))$ is the sound speed perturbation. We also assume $\delta C/C \ll 1$. These are the linearized formulations for the acoustic travel times obtained in the oceanic environment with C and u . The velocity term in the denominator of the integrand $u(x, z) \cdot n$, in Eqn. (1) accounts for changes in the apparent velocity of sound due to current, provided local shear can be ignored²⁹. In the present simulation experiment Eqn. (3) is not considered because currents are ignored in the ray tracing as the magnitude of the current shear in the ocean is typically $O(10^{-4})$ when compared with sound velocity shear which is of $O(10^{-2})$.

Eqn. (2) is integral equation with the unknown variable δC . This equation constitutes acoustic forward problem: continuous δC field is used to predict the data δT_i . The corresponding inverse problem takes data and estimates the continuous field i.e. δC . This is an infinitely under-determined problem because, values of δC must be specified at all x and z points using only a finite amount of data δT_i . So the continuous field δC will therefore be parameterized with a finite number of discrete parameters. An ocean model specifying this parameterization is supposed to be oceanographically meaningful. This has three advantages: a) the parameterization can be very efficient, b) the inverse solution becomes better determined because we are injecting our oceanographic prejudices concerning permeable structure of the fields (reducing the degree of freedom) and lastly, the model data can tell us whether the Oceanographic model is consistent with observed data or not. The two convenient model representations which have been routinely exploited by the physical oceanographic community are the Empirical Orthogonal Functions (EoFs) and the

Quasi-Geostrophic (QG) ocean modes³⁰. In this paper, we will consider EOF model studies (Appendix - A).

Stochastic Inverse

In the stochastic inverse method both the data (d) and the unknown field $[\delta C(x, z)]$ are assumed random variables having known mean and covariance functions. The best estimate $\delta \hat{C}(x, z)$ of the model parameters $\delta C(x, z) [= C(x, z) - C_0 = D]$ can then be expressed in the form

$$\delta \hat{C}(x, z) = \Sigma a_i^{-1}(x, z) \delta T_i = A(x, z) d \quad \dots (4)$$

such that the ensemble average of the square of the difference between the estimate of the unknown field $\delta \hat{C}(x, z)$ and the true field $[\delta C(x, z)]$ at each point in the medium is a minimum, i.e., a_i 's are determined such that the square of the deviation (ensemble) is a minimum at each point (x, z) . Using the Gauss-Markov theorem²⁵, a_i 's are given by

$$A(x, z) = \left\langle \delta C(x, z) \delta T_i^T \right\rangle \left[\left\langle \delta T_i \delta T_j^T \right\rangle \right]^{-1} \quad \dots (5)$$

where $\left\langle \delta C(x, z) \delta T_i^T \right\rangle$ and $\left\langle \delta T_i \delta T_j^T \right\rangle$ are the model-data and data-data covariance matrices. These are evaluated using the linearized direct problem,

$$\delta T_i = -\int_{\tau_{i0}} \frac{\delta C(x, z)}{C_0^2(z)} ds + \varepsilon_i \quad \dots (6)$$

where ε_i represents noise due to smaller scale phenomena and measurement errors, assumed to have zero ensemble average and to be uncorrelated with the mesoscale sound velocity fluctuations. Using Eq. (6) the model-data and data-data covariance matrices can be expressed as

$$\begin{aligned} \langle \delta C(x, z) d^T \rangle &= \langle \delta C(x, z) \delta T_i^T \rangle \\ &= \int_{\Gamma_{oi}} \frac{\langle \delta C(x, z) \delta C(x', z') \rangle}{C_0^2(x', z')} ds' \quad \dots (7) \\ &= \int_{\Gamma_{oi}} \frac{\left[\left(\sum_i^p a_i(x) u_i(z) \right) \left[\sum_{i=1}^p a_i(x') u_i(z') \right] \right]}{C_0^2(x', z')} \frac{dx'}{\cos \theta'} \end{aligned}$$

$$\begin{aligned} \langle d d^T \rangle &= \langle \delta T_i \delta T_j^T \rangle \\ &= \int_{\Gamma_{0j}} \frac{dx''}{\cos \theta''} \int_{\Gamma_{0i}} \frac{\left[\sum_i^p a_i(x') u_i(z') \right] \left[\sum_{i=1}^p a_i(x'') u_i(z'') \right]}{C_0^2(x', z') C_0^2(x'', z'')} \\ &\times \frac{dx'}{\cos \theta'} \quad \dots (8) \end{aligned}$$

where $\gamma_{ij} = \langle \epsilon_i \epsilon_j \rangle$ is the error covariance matrix $(x', z'), \theta'$ and $(x'', z''), \theta''$ are the coordinates and angles of the *i*-th and *j*-th along rays respectively. In Eqns. (7) and (8), the integrations are carried out along the eigenrays (Γ_{0i} and Γ_{0j}). In the above equations, $u_i(z)$ are the vertical EOF modes (column vectors of *U*) of covariance matrix $D = U \Gamma V^T$ (SVD form) and horizontal modal amplitudes $a_i(x)$ are obtained (Appendix-A) as follows:

$$a_i(x) = \sum_{n=1}^p \delta C(x, z_n) u_i(z_n) \quad \dots (9)$$

i = mode index, *n* = layer index, *p* = factor index ($\leq r = \text{rank of } D$)

For each point in a given region, the coefficients $a'_i(x, z)$ are determined from the eigenrays and operated on the travel time perturbations to objectively estimate the model parameter $[\delta \hat{C}(x, z)]$. This procedure permits a continuous representation of the unknown field. The data-data and model-data covariance matrices are determined for the reference sound velocity distribution with a suitably selected source-receiver configuration. Using these matrices the sound velocity field $[\delta \hat{C}(x, z)]$ of the real ocean is obtained for the given travel time perturbations (δT).

The required components of OAT are discussed below and they are: 1) preparation of available data, 2) acoustic model simulation of forward problem in reference ocean, 3) optimal estimation of sound velocity perturbations from travel time perturbations (inverse problem) and finally 4) the interpretation of results for oceanographic applications.

Data collection

The hydrographic survey was carried out on board ORV Sagar Kanya during 21-29 July 1984, and

occupied a total number of 42 CTD stations near the western boundary of North Bay of Bengal (Fig. 2). From CTD data, sound velocity has been computed following *Chen and Millerio*³¹ at standard depths.

Results and Discussion

Sound velocity field

In order to examine the variability of sound-velocity in the presence of cold core eddy, the sound velocity structure $C(x, z)$ across the eddy track parallel to the coast (Fig. 2) is presented along with vertical profiles at stations #23, #33, #40, #56 and #61 (Figs. 3 & 4). All the profiles are similar in shape having a well defined deep sound channel and a smaller duct near the surface (Fig. 3). The sonic layer depth, which is the depth of near-surface sound-velocity maximum, changed abruptly by about 20 m across the eddy. At the surface the sound velocity varied by 8 ms^{-1} with a decreasing trend from south to north. This variation is brought about by the presence of low saline cold water in the northern Bay of Bengal (associated with freshwater discharge), reducing the sound velocity value and the comparatively high saline warm water present in the southern side giving rise to higher sound velocity value. Below the surface, the eddy is clearly discernible from the up tilt of $1500\text{-}1520 \text{ ms}^{-1}$ sound velocity isopleths (Fig. 4).

The presence of eddy brings about a reduction in the sound-velocity. At 60 m depth, the sound velocity reduces by 4 ms^{-1} across the eddy. A maximum reduction occurs at 120-140 m layer, at the centre of the eddy (#40) where the sound-velocity drops up to

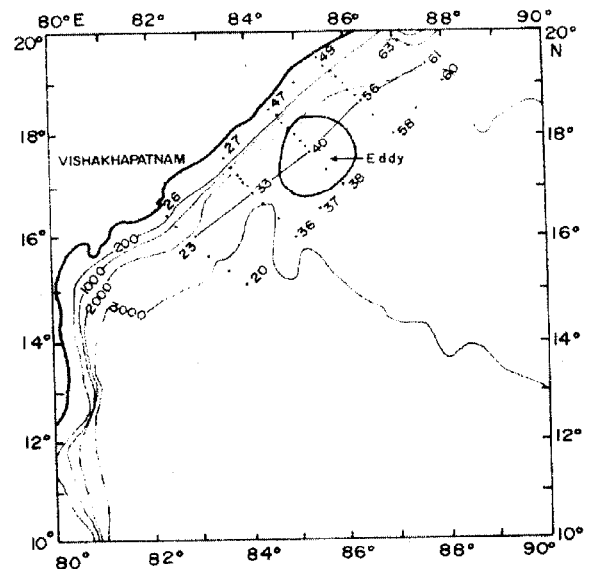


Fig. 2—Station locations

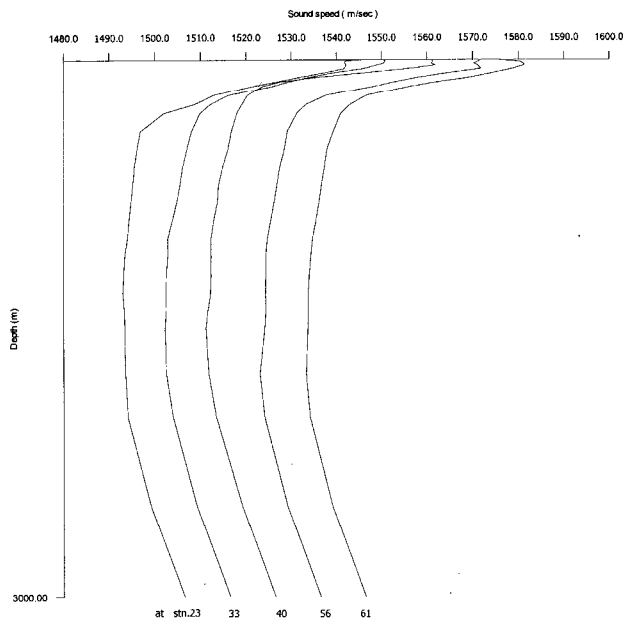


Fig. 3—Sound velocity profiles along parallel track (Fig. 2) (The consequent profiles are drawn by incrementing 10m/sec in horizontal direction)

14 ms⁻¹. Below 300 m depth the variability in sound-velocity is less than 2 ms⁻¹. The effect of cold core eddy is to reduce the ambient sound-velocity by approximately 10 ms⁻¹, associated with this the depth of channel axis and axial velocity also undergone changes (Table 1).

In general, the depth of deep sound channel axis increases from south to north along the track parallel to the coast. However, below the cold core eddy, the channel axis depth remains constant (1600 m). Accordingly the sound velocity at the channel axis below the eddy reduces by about 1.5 ms⁻¹. The conjugate depth is decreasing from south to the center of the eddy and then onwards again it starts increasing. This indicates that cold core cyclonic eddy, uplift depth isopleths by 75 m with reference to normal conditions (Table 1). The importance of monitoring such mesoscale cyclonic eddies and their role of such processes in enhancing surface ocean productivity has been extensively studied³² in the past. After utilization of OAT principle and stochastic inverse, later it was proved that it is possible to monitor such cyclonic eddies to some extent even under depth-limited environment of tropical waters. Unlike cyclonic eddies, in the case of anticyclonic eddies, (i.e., have downward-tilting isopycnal surfaces in the interior) leading to little expected change in

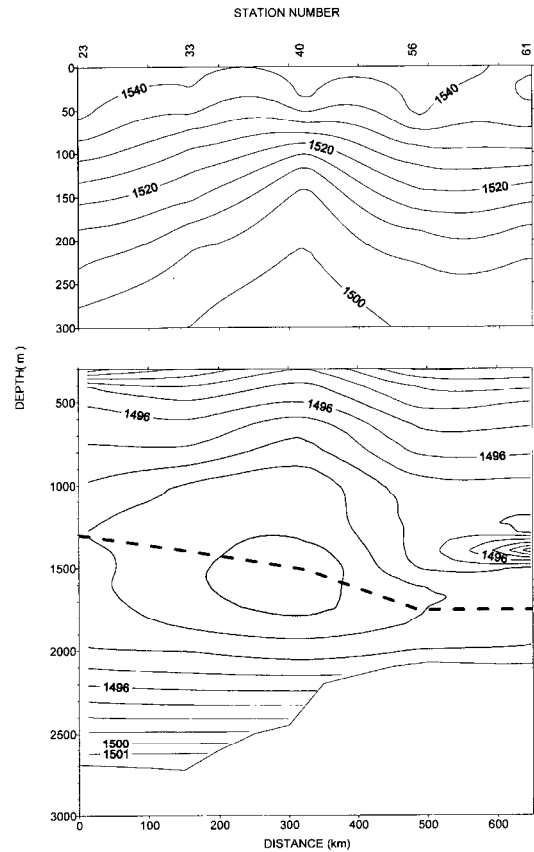


Fig. 4—Vertical sound velocity (m/sec) structure across the eddy parallel to the Coast ----- indicates the depth of SOFAR channel axis

productivity. However this phenomenon has important role in studying the dynamics of interior water. Anyhow there is no limitation to monitor the anticyclonic eddies, below the conjugate depth, using OAT principle, but in the present study, it is not the case. In our simulation we have used the knowledge of the sound velocity perturbation itself to compute the covariance.

In order to use the stochastic formalism, it is necessary to define a mean state of $C_0(z)$ for the sound-velocity and the expected covariance around this basic state. Because we are interested in deriving reliable snapshots of the evolution of the sound-velocity anomalies $\delta C(x, z)[= C(x, z) - C_0 = D]$ due to mesoscale dynamics, we are more interested in the minimum variance properties of the estimator. For this reason, the basic state need *only* be specified reasonably close to the true state to avoid problems *due to* linearization. It means that any archived estimate of the local mean sound-velocity is adequate

Table 1—Sound channel parameters

St No.	Latitude (⁰ N)		Longitude (⁰ E)		Sound channel depth (m)	Sound velocity at channel depth (m/sec)	Conjugate depth (m)	Sound velocity at conjugate depth (m/sec)
	Deg	Min	Deg	Min				
23	15	59.84	82	54.94	1350	1493.04	250	1508.46
33	17	00.26	83	59.80	1400	1492.00	200	1506.09
40	17	40.12	85	19.76	1500	1491.11	125	1507.52
56	18	40.05	86	17.85	1750	1493.02	150	1518.48
61	19	21.98	87	39.96	1750	1493.21	150	1516.45
Reference Profile	-	-	-	-	1500	1493.07	200	1507.51

to use as basic state, so that the closer the assumed mean state to the true mean, the smaller the variance around the mean will increase the effectiveness of the estimator.

For the initial estimate to the numerical experiment, following a simple average $C_0(z)$ be written as:

$$C_0(z_k) = \frac{1}{n} \sum_{j=1}^n C_j^1(x_j, z_k) \quad \dots (10)$$

n is no of profiles,

where sound velocity profiles $C'(x, z)$ that are computed from Levitus hydrographic data along the same track (shown in Fig. 2) is chosen to the basic state. The basic state is taken to be stationary and horizontally homogeneous, [i.e., $C^l(x, z, t) = C_0(z)$], both for simplicity and also the data available to date are inadequate to support any assumptions to the contrary.

The estimate of covariance for the sound-velocity anomaly [$C(x, z) - C_0(Z) = D$] is also derived from observed eddy profiles and Levitus archived data (of the same track) (Fig. 2), and then used in the forward problem to calculate the expected data-data covariance matrix. The decomposition into vertical modes $\{u_i(z)\}$ with horizontally varying amplitudes $\{a_i(x)\}$ is described in the Appendix-A. This model is used throughout the inversions to follow:

$$\delta C(x, z) = \sum_{i=1}^r u_i(z) v_i(x) l_i^2 \quad \dots (11)$$

r = rank of D

The modes chosen as basis (i.e. depth-dependent set $s(z)$; range – dependent set $s(r)$ that are defined in Appendix-A) are the Empirical Orthogonal Functions (EOF) of sound velocity variation shown in (Fig. 2). It

is also more logical to use the historical averaged sound velocity profile as a reference, rather than the average of the observed eddy profiles. In the actual experiment, basis supposed to be chosen before the data available by actually conducting the experiment, so that the model would be independent of the traditional measurements made during the experiment. However traditional measurements made are useful for validation.

In deriving the EOF modes, we have tacitly assumed flat bottom geometry of the ocean, for which the modes are complete and mutually orthogonal set. In the present study area, ocean bottom is not actually flat (Fig. 2). EOF expansion cannot be made, and therefore one has to see for alternatives. To circumvent this difficulty, we employ the artifice of “false bottom” located at the deepest bathymetry point³³, to fill the values of sound velocity. While employing the “false bottom” method, it doesn’t affect the top layer, as sound velocity variability with reference to subsurface eddy is negligible.

EOF modes

This method has been widely used in many types of distributions by different workers. The geometrical interpretation of this method has been briefly explained by *Wiggins*³⁴. It is important to point out that EOF may or may not have physical significance or interpretation but depends certainly on the data examined. However, various researchers from different disciplines employed the technique for different purposes. *Stidd*³⁵ used eigen vectors to represent the seasonal variation of rainfall over Nevada and found that the first three eigen vectors, in order of importance have features in common with the three natural cycles of precipitation. This technique was used^{36,37} to beach data and attributed the first three eigen vectors to beach profiles, mean seasonal

cycles and high frequency random oscillations respectively. *Ramana Murty et al.*³⁸ used this method to grain-size data to identify the different energy environments along central west coast of India. First two modes represent the barotropic and baroclinic modes of sound velocity structure. *Cornuelle*²² used this technique and derived EOF modes from historical hydrographic data to construct the total data – data covariance matrix while formalization of stochastic inverse. He explained that EOFs allow variance in the upper layers of the ocean, presumably due to seasonal effects.

Computational procedure of vertical and horizontal EOF's of perturbation matrix D of order $(m \times n)$ and their horizontal modal amplitudes are detailed in the Appendix-A for two cases $m < n$ and $m > n$. In the present case we have $n = 5$, vertical profiles (Fig. 2) each containing $m=28$ horizontal layers and then D^T will be 5×28 matrix. Each column of the matrix will be a profile of sound velocity perturbations from the background $[C_0(z)]$ and comes under the case $m > n$. The computed eigenvalues (l_i) arranged in the descending order in the diagonal matrix of Γ and percentage contribution of each eigenfunction (eigenmode) using closeness approach (Eqn. A8) are shown in Fig. 5. The computed depth-dependent eigenmodes of $s(z)$ (i.e., $u_i, i=1,n$), range-dependent eigenmodes of $s(r)$ (i.e., $v_i, i=1,n$) and horizontal modal amplitudes $[a_i(x), i=1,n]$ (using Eqn A7) are shown in Fig. 5 and Table 2. Column vectors $u_i (i=1, \dots, 5)$ of $s(z)$ of corresponding eigenvalues l_i (measure of variance D accounted for mode i) having 28 elements and each element has a value indicating amplitude which explains sharing contribution of it's variance mode i . The vectors u in the $s(z)$ represents the trend or direction of depth-spatial common features contained in perturbation matrix D . Its corresponding eigenvalues l_i represents energy level³⁴. In a similar manner the components of vectors in set $s(r)$ can also be explained.

The percentage contribution of individual components of $s(z)$ and $s(r)$ are computed through closeness ratio approach (using Eqns. A9 & A10) and are shown in Table 3. From this table, the first four eigenfunctions of $s(z)$ and $s(r)$ account for more than 98% of variance, relatively dominated by the first function alone (60.42%). The first depth-dependent eigenfunction u_1 of $s(z)$ contribute 60.42% of the total distribution showing maximum variance between the

depths 50 – 300 m (vertical width of eddy) and is less at its top and below layers of the ocean (Fig. 4 & Table 3a). Maximum dominant contribution (modal value) of u_1 is 9.46% (Table 3) of total distribution (61.42%) at depth 125m indicating conjugate depth (Table 1) of sound velocity of cold core eddy. The first range – dependent eigen function v_1 of $s(r)$ contribution is 60.42% of total distribution showing maximum variance at stations #23 and #40 and relatively less contribution at the other stations

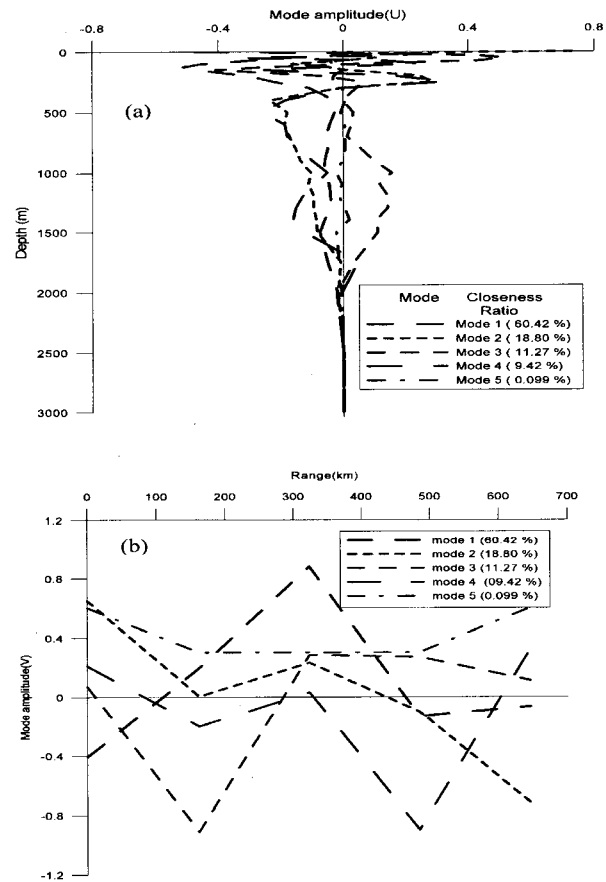


Fig. 5— (a) Vertical (U) distribution of empirical eigenfunction of sound velocity perturbation ($\delta C(x,z)$); (b) Horizontal (V) distribution of empirical eigenfunction of sound velocity perturbation ($\delta C(x,z)$)

Table 2—Horizontal modal coefficients ($a_i(x)$)

Mode No.	Station No.				
	St. 23	St. 33	St. 40	St. 56	St. 61
(i)	$a_i(1)$	$a_i(2)$	$a_i(3)$	$a_i(4)$	$a_i(5)$
1	-11.85	5.70	25.62	-3.83	-1.90
2	5.88	0.039	2.09	-0.92	-6.49
3	0.38	-4.95	1.54	1.46	0.60
4	0.94	-0.91	0.14	-4.08	1.48
5	0.03	0.014	0.014	0.014	0.03

(Fig. 5a & Table 3b). Maximum dominant contribution (modal value) of v_1 , is 31.65% (Table 3b) of total distribution (61.42%) at station #40 indicating centre of the eddy. All the depth-dependent eigenmodes of $s(z)$ have higher values in the top vertical layers of the ocean and somewhat less in the middle layers and no variation below 2000 m depth. From figure (5b), one can infer that the shape of eigenmodes is similar, but in Table 2, $\{a_i(x)\}$ are amplified by the energy levels of times v_i . A great advantage of this representation is that the EOF's are the most efficient representation available in the sense that one needs least number of modes to account for a given percentage of the variance between the actual field and its representation. For a real ocean wavenumber spectrum, the modes sum can be truncated since the higher modes will contain little

energy. As the ocean does have a red spectrum, this reduces the number of modes needed and, the more important number of $a_i(x)$ one has to store. The following resolution matrices tell us which combination of the data are well resolved³⁹.

Data Resolution Matrix ($U_p U_p^T$)

The data resolution matrix is an identification of the information density of the data kernel, i.e. it indicates which data contribute independent information to the solution. The computed diagonal elements of the data resolution matrix in the $s(z)$ base are shown in the Table 4a. Higher values are found to be at depths 75 -300m with one mode ($p=1$) with contribution of 60.42%. Resolution has improved at depths between 200-250m and also deeper depths considering 2 modes ($p=2$) with contribution of 79.22%, but no gain at depths between 77-150m. Considering 4 modes ($p=4$), resolution improved, but not much, up to depth of 30m. For modes $p=5$, it is observed that there is no change in the resolution from $p=4$.

Model Resolution Matrix ($V_p V_p^T$)

Model parameter resolution is an indication of how perfectly and independently each model parameter is determined. The diagonal elements of model parameter resolution matrix (Table 4b) give a clue as to how well the individual model parameters in the $s(r)$ base are resolved. A value of unity indicates perfectly resolved parameter, whereas a smaller value means inadequate resolution. From Table 4b, it can be seen that parameter resolution is found to be higher at two stations namely Stn #40 (center of eddy) & #23, due to first mode ($p=1$) itself with contribution of 31.64% and 14.64% respectively (Table 3b). Considering the four modes ($p=4$), resolution at stations #33, 40 & 56 has improved well with 99% contribution, but relatively less improved at Stn #23 & 61 respectively.

Table 3(a)—Percentage contribution of individual component data space $s(z)$

Depth (m)	$u_1\%$	$u_2\%$	$u_3\%$	$u_4\%$	$u_5\%$
0	-0.548	3.851	0.053	-1.055	0.002
10	-0.087	0.704	0.18	-0.084	0.001
20	-0.304	0.383	0.251	0.521	-0.001
30	-0.133	0.418	1.37	0.411	-0.001
50	-3.163	0.556	1.662	-0.709	0
75	-5.772	-0.039	1.434	0.296	-0.003
100	-8.411	-0.866	0.208	0.551	-0.002
125	-9.464	-0.295	-0.764	-0.059	0
150	-8.641	0.033	-1.329	-0.579	0
200	-5.618	1.303	-0.227	0.357	-0.002
250	-4.082	1.512	0.211	0.76	-0.002
300	-2.012	-0.041	0.139	-0.014	0
400	-0.542	-1.235	-0.004	-0.416	0.001
500	-0.503	-0.946	0.107	-0.579	-0.001
600	-0.789	-0.991	0.085	-0.417	0
700	-1.02	-0.911	0.041	-0.398	0
800	-0.914	-0.804	0.184	-0.294	0
900	-1.098	-0.728	0.32	-0.224	0
1000	-1.155	-0.551	0.507	-0.115	-0.001
1100	-0.846	-0.591	0.379	-0.202	0
1200	-0.763	-0.505	0.463	-0.288	-0.001
1300	-0.74	-0.501	0.462	-0.34	0
1400	-1.12	-0.461	0.348	-0.359	0.001
1500	-1.398	-0.444	0.36	-0.279	-0.001
1750	-0.94	-0.044	0.113	0.104	0.066
2000	-0.357	-0.089	-0.068	-0.01	0
2500	0	0	0	0	0
3000	0	0	0	0	0
Total	60.42	18.8	11.27	9.42	0.09

Table 3(b)—Percentage contribution of individual components of model space $s(r)$

St. No	$v_1\%$	$v_2\%$	$v_3\%$	$v_4\%$	$v_5\%$
23	-14.637	7.171	0.475	1.182	0.026
33	7.053	0.047	-6.247	-1.134	0.013
40	31.645	2.55	1.944	0.176	0.013
56	-4.733	-1.125	1.846	-5.084	0.013
61	-2.352	-7.906	0.758	1.845	0.026
Total	60.42	18.8	11.27	9.42	0.09

Table 4(a)—Diagonal elements of data resolution ($U_p U_p^T$) for each depth for factor $p = 1$ to 5

Depth (m)	Modes				
	1	2	3	4	5
0	0	0.53	0.54	0.76	0.76
10	0	0.02	0.02	0.02	0.02
20	0	0.01	0.01	0.07	0.07
30	0	0.01	0.18	0.22	0.22
50	0.03	0.04	0.3	0.4	0.4
75	0.1	0.1	0.29	0.31	0.31
100	0.21	0.21	0.24	0.3	0.3
125	0.26	0.26	0.32	0.32	0.32
150	0.22	0.22	0.39	0.45	0.45
200	0.09	0.15	0.16	0.18	0.18
250	0.05	0.13	0.14	0.25	0.25
300	0.01	0.01	0.01	0.01	0.01
400	0	0.06	0.06	0.09	0.09
500	0	0.03	0.03	0.1	0.1
600	0	0.04	0.04	0.07	0.07
700	0	0.03	0.03	0.07	0.07
800	0	0.03	0.03	0.05	0.05
900	0	0.02	0.03	0.04	0.04
1000	0	0.01	0.04	0.04	0.04
1100	0	0.01	0.03	0.04	0.04
1200	0	0.01	0.03	0.05	0.05
1300	0	0.01	0.03	0.05	0.05
1400	0	0.01	0.02	0.05	0.05
1500	0.01	0.01	0.02	0.04	0.04
1750	0	0	0	0.01	1
2000	0	0	0	0	0
2500	0	0	0	0	0
3000	0	0	0	0	0

Table 4(b)—Diagonal elements of model resolution ($V_p V_p^T$) for each station for factor $p = 1$ to 5

Range (km)	Modes				
	1	2	3	4	5
0.00	0.17	0.59	0.59	0.64	1.00
161.62	0.04	0.04	0.87	0.91	1.00
323.23	0.77	0.83	0.91	0.91	1.00
484.83	0.02	0.03	0.10	0.91	1.00
646.49	0.00	0.52	0.53	0.64	1.00

Eigen Rays

In order to understand the effect of cold core eddy on acoustic propagation, a range independent acoustic ray tracing is utilized. The ray tracing⁴² is carried out using the mean (left panel of Fig. 6a) as well as the eddy profiles (Fig. 3) for a range of 650 km, with the same source-receiver configuration kept at a depth of

1500 m in the SOFAR channel. The nature of mean profile (left panel in Fig. 6a) is depth limited since its bottom velocity is less than the surface velocity. The conjugate depth of this profile is 200m (column 8 of Table 1). So in the present acoustic simulation experiment under such a depth limited environment, emitted sound pulses never enter into the top 200m layer from any source to receiver kept in the SOFAR channel (Table 1). Eigenrays between the source and receiver for unperturbed ocean are shown in Fig. 6a (right panel) that also reveals the same conclusion. In order to know the effect of sub-surface cold core eddy on the propagation, ray paths are plotted (Fig. 6b) at the neighboring eddy location under unperturbed and perturbed conditions. In Fig. 6b2, eigenrays are trapped and uplifted 75m due to up tilt of 1500-1520 ms^{-1} sound-speed isopleths (Fig. 4) in the region of cold core eddy as compared to unperturbed condition as shown in the Fig. 6b1. Here cyclonic eddies played a significant role in the interaction with the surface waters and in turn acoustic field, by raising the thermocline locally. It is evident from Fig. 6b2 that further scanning of traced rays (in contrast to unperturbed condition, Fig. 6b1) has taken place in the water column above the conjugate depth. Due to the displacement of eigenrays by cold core eddy, travel times (with reference to mean) are delayed (column 6 of Table 5 & Fig. 7). To perform inversion of the travel time data, each arrival must be associated with a particular ray path corresponding to the reference as well as to the eddy profile. This identification is achieved by comparing the simulated arrivals for both mean and eddy in the time domain (Fig. 7a & Table 5). Table 5 presents the characteristics of each of the 8 eigenrays. The columnwise ray nomenclature in Table 5 is detailed as a footnote. The columns 7 to 12 of Table 5 explains number of upper (p^+) and lower (p^-) ray turnings, number of top (p_t^+) and bottom (p_b^-) ray bonks, and total number of ray turnings and bonks respectively. This information can be used as the ray identifier.

There are four classes of rays 1) *R/R* (purely refracted both above and beneath the axis, $p_t^+ = p_b^- = 0$) 2) *SR/R* (surface reflected and refracted, $p_t^+ \neq 0, p_b^- = 0$), 3) *R/BR* (refracted and bottom reflected, $p_t^+ = 0, p_b^- \neq 0$) 4) *SR/BR* (surface and bottom reflected, $p_t^+ \neq 0, p_b^- \neq 0$). It is

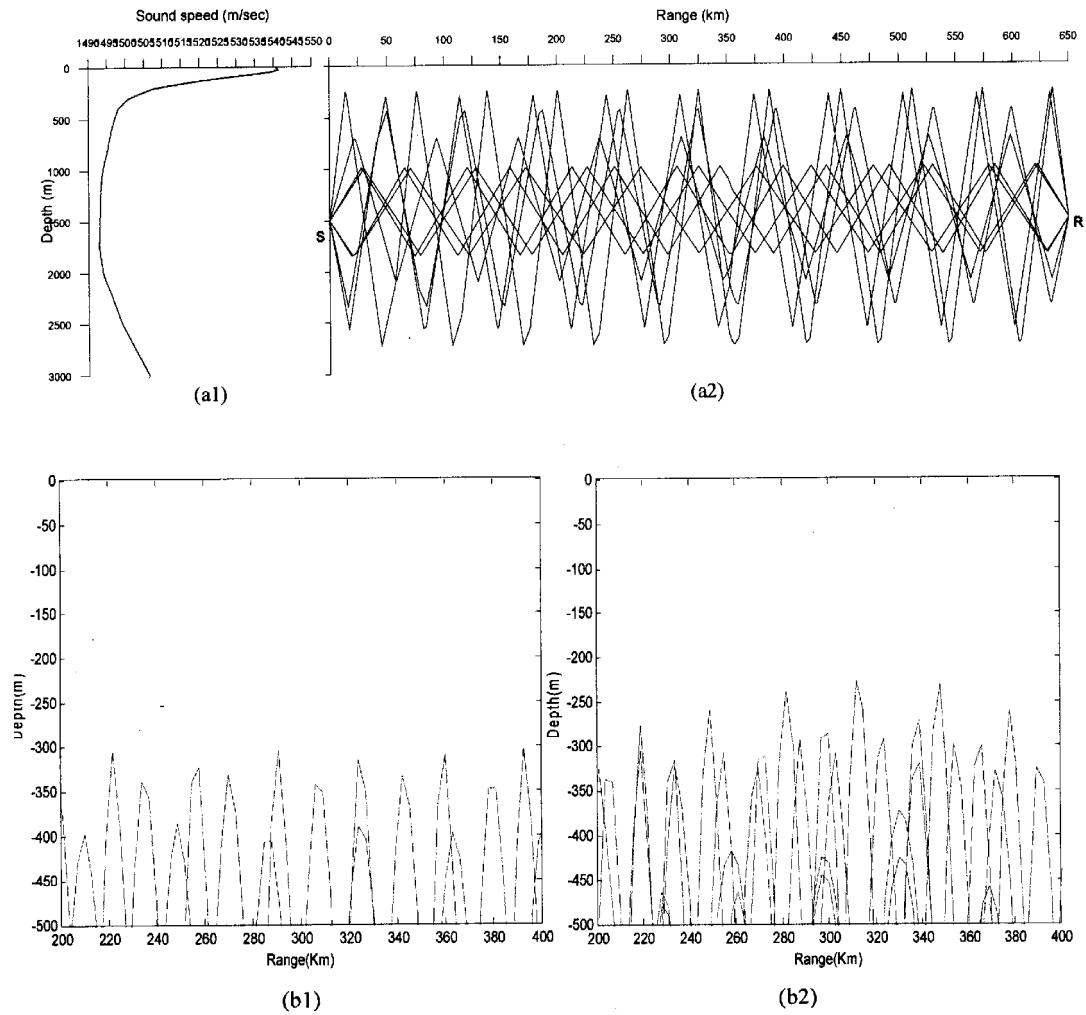


Fig. 6— (a1). Mean sound velocity profile ($C_\theta(z)$) constructed from Levitus data along parallel track (Fig. 2) (a2). Eigenray plot for a source and receiver located at 1500m depth over a range of 650km. (b1) Ray paths in the reference ocean ($C_\theta(z)$) at cold core eddy location. (b2) Ray paths in the presence of cold core eddy location.

Table 5—Acoustic ray parameters for source depth = 1500 m, receiver depth = 1500 m and range =650 km.

S. No.	θ_0 (deg)	θ_r (deg)	T (sec)		Travel time anomaly (sec) (δT^M)	P^+	P^-	P_t^+	P_b^-	$P^+ + P^-$	$P_t^+ + P_b^-$	-db	
			Reference	Presence of Eddy								Reference	Presence of Eddy
1	6.52	-6.52	435.8272	435.8610	-0.03380	11	11	0	0	22	0	108.3	112.2
2	4.15	-4.16	435.5750	435.6500	-0.07500	10	10	0	0	20	0	106.9	116.4
3	3.08	3.09	435.5202	435.5493	-0.02910	9	10	0	0	19	0	119.3	118.7
4	0.86	0.86	435.4674	435.3148	0.15260	7	8	0	0	15	0	113.6	116.4
5	0.76	-0.80	435.4582	435.3060	0.15220	7	7	0	0	14	0	114.3	123.4
6	-0.71	0.71	435.4539	435.2991	0.15480	7	7	0	0	14	0	114.1	120.8
7	-4.66	4.69	435.5539	435.6272	-0.07330	10	10	0	0	20	0	109.8	116.3
8	-5.75	-5.81	435.6700	435.7369	-0.05790	11	10	0	0	21	0	117.1	114.9

Θ_0 - ray launching angle at source, Θ_r - ray angle at receiver, T – travel time, p^+ - number of upper turning points, p^- - number of lower turning points, p_t^+ – number of top bonks, p_b^- – number of bottom bonks, $\delta \Theta$ – acoustic intensity loss

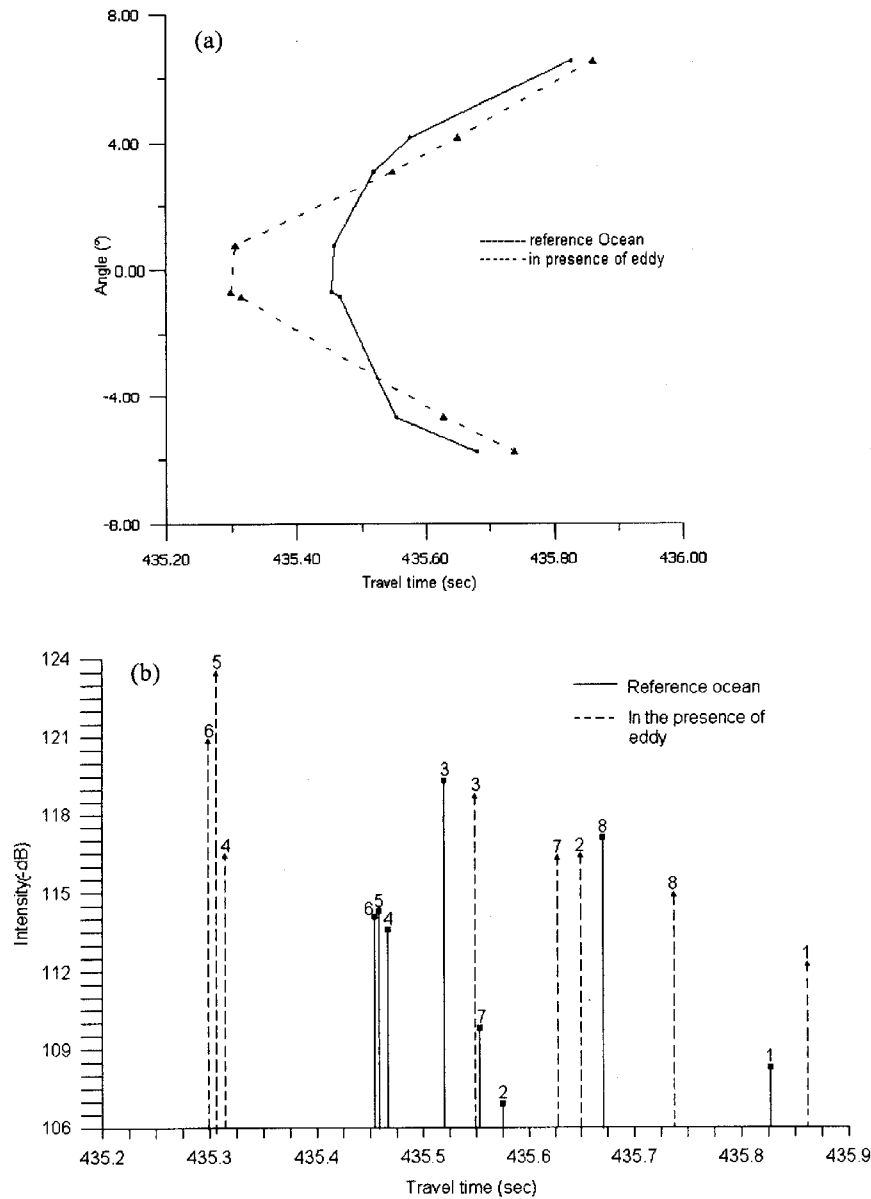


Fig. 7— (a) Travel time versus eigen ray angle for the reference and eddy profiles (b) Comparison of predicted arrival pattern obtained from reference ocean ($C0(z)$) and eddy profiles. (The arrivals are labeled and identified in Table 5).

interesting to note that in the Bay of Bengal, long-range acoustical transmission paths are mostly refracted/bottom-reflected, (R/BR), and refracted/refracted, (R/R). In the present study, we have considered the R/R category rays among all possible above said classes to avoid bottom losses (Table 5).

Ray arrival pattern

The travel times of eigenrays are determined by two factors viz., the ray path length and the sound-velocity along the path. The flat rays with small initial

angles travel along shorter paths in lower sound-velocity region. On the other hand, the steep rays, which have larger initial angles, travel in faster sound-velocity regions but over greater path lengths. In general, the path lengths of steep rays in the top layer are less as compared to deeper layers. The combined effect of path length and sound-velocity on the ray travel times shown as a function of launch angle in Fig. 7a. The predicted arrival pattern depicts the typical characteristics of the Bay of Bengal sound propagation namely the early arrival clusters of near –

axial flat angle rays (+0.85° to -0.85°) and the later arrivals of deep-turning rays (*R/R*). This type of arrival pattern arises due to the weak acoustical wave guide nature of the Bay of Bengal, contradictory to general pattern of other waters⁴⁰. It is discernible from the diagram that although the arrival angle (Fig. 7a) remains the same to a large extent for both the profiles, the arrivals are delayed by about 20-75 ms (milliseconds) in the presence of the eddy for steep angle rays (column 6 of Table 5). The travel times of flat angle rays also showed delays due to channel depth variation (400 m from south to north, as shown in Fig. 4), and also weak acoustic wave guide nature (Table 5). In the present simulation, one can expect that the travel time perturbations of steep angle rays which travel through eddy are supposed to show more as compared to flat angle rays, for a long range of 650km. However slowness, of steep angle rays in the present case are due to less transgressed in the top layer (Table 5).

Acoustic intensity

The computed intensity of eigenrays (using the ray tube method) at the receiver end⁴² shows the loss associated with steep angle rays through the average field is about 112.28 dB, while that through the eddy field is about 115.7 dB (Fig. 7b & columns of 13 & 14 of Table 5). The flat angle rays (+0.85° to -0.85°), which do not sample the eddy; undergo average intensity loss of 114.05 dB and 119.25 dB for unperturbed and perturbed conditions respectively (Fig. 7b & Table 5).

Inversion

Building the estimates

For each point in a given region, the coefficients $a_i^j(x,z)$ (in Eq.4) are determined from the eigenrays and operated on the travel time perturbations(d) to estimate the model parameter $[\delta\hat{C}(x, z)]$ objectively. This procedure permits a continuous representation of the unknown field. The data-data and model-data covariance matrices are determined for the reference sound velocity distribution with a suitably selected source-receiver configuration. Using these matrices the estimated sound velocity field $[\delta\hat{C}(x, z)]$ of the real ocean $[\delta C(x, z)]$ is obtained for the given travel time perturbations (δT).

Once the model covariance (the unknown field - in this case, the sound velocity anomaly) is obtained, the model-data covariance ($\langle \delta C(x, z)d^T \rangle$) of order ($M \times 1$) and data-data covariance matrices ($\langle dd^T \rangle$) of order

($M \times M$) can be constructed as described in the above theory (Eqs.5-9). In the present example, model-data covariance matrix ($\langle \delta C(x, z)d^T \rangle$) is of order ($M \times 1$) where $M=8$ is the number of identified eigenrays (Table 5). For example, computation of each element in matrix ($\langle \delta C(x, z)d^T \rangle$) is generated by evaluating the single integration (Eq. 7) along the i -th identified eigenray (columns 7-12 of Table 5). The integrand in the Eq.7 consists of a point (x, z) in the vertical domain (where model parameter estimation $\delta\hat{C}(x, z)$ to be computed), refractive index, vertical (U) and horizontal ($a_i(x)$) i.e., EOF modes. While performing integration, the cubic spline interpolation is carried out to evaluate vertical functional values of (U) of $s(z)$ distribution and horizontal modal amplitudes ($a_i(x)$) of $s(r)$ for all modes along i -th eigenray co-ordinates⁴² [$x^i(s), z^i(s)$] (where s is the distance along ray). The model-data covariance is constructed for mapping 5 points in the horizontal (at the station locations of the 5 CTD casts in the survey). This is carried out for easy comparisons between the estimates of sound velocity from assumed acoustic data and those calculated from the CTD stations. Note that the changes to the output of the estimator affect only the rows of the model-data covariance matrix. Similarly data-data covariance matrix ($\langle dd^T \rangle$) can be computed.

In the present example, data-data covariance matrix ($\langle dd^T \rangle$) is of the order ($M \times M$) where $M=8$ is the number of identified eigenrays (Table 5). For example, computation for each element in matrix ($\langle dd^T \rangle$) is generated by evaluating the double integration (Eq. 8) along both the i -th and j -th identified eigenrays (Table 5).

The data-data covariance matrix is fixed by the data available in the experiment or assumed simulation, and therefore does not change when a new output is desired. When any particular field or distribution of mapping points are desired, one needs only to compute the appropriate model-data covariance matrix and then multiply it by the inverse of the data-data covariance matrix, which is computed once and saved. Here Generalized Inverse Operator (GIO) (i.e., $A_g^{-1} = V_p \Gamma_p^{-1} U_p^T$) of the data-data covariance matrix ($\langle dd^T \rangle$)⁻¹ is built using SVD employing eigenvalues technique⁴¹. Here p indicates the number of factors used in SVD, which is less than or equal of the rank of the matrix ($\langle dd^T \rangle$) (i.e., $p \leq M$, where M is the number of eigenrays). Also, U_p ,

and V_p are the column eigenvectors of the matrix $\langle \langle dd^T \rangle \rangle$ of U and V . Γ_p is the diagonal matrix of the matrix $\langle \langle dd^T \rangle \rangle$. The elements of diagonal matrix (eigenvalues) arranged in descending order and corresponding closeness ratio is presented in the Table 6. The SVD provides a simple framework for determining how well the inverted model parameters fit the data, and how closely the model parameter estimates the true values. The larger eigenvalues determine the large scale (gross) features of the problem, while the smaller eigenvalues correspond to

small scale or higher frequency features. Then Eq.5 becomes.

$$A(x, z) = \langle \delta C(x, z) \delta T_i^T \rangle A_g^{-1} \dots (12)$$

Using this matrix $A(x, z)$ the estimated sound velocity anomaly field $[\delta \hat{C}(x, z)]$ (Eq.4) of the real ocean $[\delta C(x, z)]$ for different factors p ($=1$ to 5), is obtained for the given travel time perturbations (δT) of Table 5. Fig. 8 gives the comparison between the tomographically reconstructed sub-surface cold core eddy field with that of observed ones (right of lower panel in Fig. 8). Even three factors (contribution of 86%, Table 6) are more than sufficient to objectively resolve the sub-surface eddy (gross features), whereas for fine structures, at least five factors are needed.

Present, OAT's simulation experiment results reveal that one can objectively map/monitor the even small mesoscale sub-surface eddies by stochastic inverse technique keeping source and receiver in the SOFAR channel separated by probably for larger distances also under such a depth-limited environment of Bay of Bengal.

No.	Eigenvalue	Closeness Ratio (%)
1	0.709	44.97
2	0.610	34.19
3	0.283	7.15
4	0.267	6.38
5	0.227	4.62
6	0.154	2.11
7	0.071	0.45
8	0.037	0.13

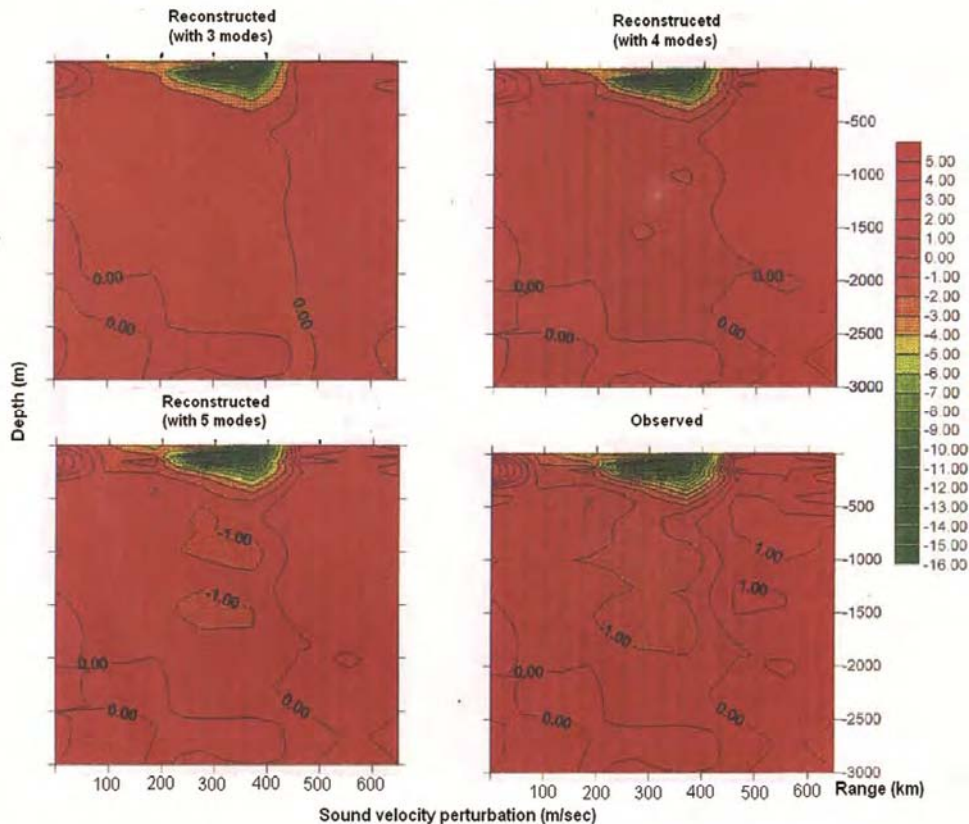


Fig. 8—Tomographic inversion of a cold core eddy in the Bay of Bengal (ORV Sagar Kanya during 21 – 29 July, 1984)

Table 7—Diagonal elements of resolution of data-data matrix [$\langle \mathbf{d}\mathbf{d}^T \rangle_p \langle \mathbf{d}\mathbf{d}^T \rangle_p^T$] for each angle for factor $p = 1$ to 8

S.No.	Eigen Ray angle (θ_0^0)	Modes							
		1	2	3	4	5	6	7	8
1	6.52	0.48	0.98	0.99	0.99	0.99	1	1	1
2	4.15	0	0	0.01	0.02	0.05	0.12	0.46	0.7
3	3.08	0	0	0.03	0.04	0.05	0.12	0.53	0.89
4	0.86	0	0	0.33	0.34	0.77	0.95	0.99	1
5	0.76	0.01	0.01	0.15	0.36	0.42	0.87	1	1
6	-0.71	0.34	0.75	0.8	0.96	0.96	0.99	1	1
7	-4.66	0	0	0	0	0.01	0.03	0.04	0.41
8	-5.75	0.01	0.01	0.39	0.43	0.86	0.97	1	1

For the assessment of the validity of the layering in the model used for inversion, it is essential to look at the model and data resolution matrices, but in the present case, both are the same. Here after we call them resolution matrix [$\langle \mathbf{d}\mathbf{d}^T \rangle_p \langle \mathbf{d}\mathbf{d}^T \rangle_p^T$]. The diagonal elements of this matrix for different factor $p=1$ to 8 are presented in the Table 7. A value of unity indicates contribution of information independent of the other observations. Among all the rays, the most independent information is contained by 6.52° ray. Because of propagation of rays in homogenous medium, poor information resolution (resulting from sampling nearly the same ocean region) was noticed (Table 7). Flat angle rays show maximum values in the vicinity of the sound velocity layer (Table 7, sl.no.4). This is due to the nature of the SOFAR channel where ray bending takes place towards the sound velocity minimum focusing an envelope.

Conclusion

In this paper, we report the acoustic characteristics of a sub-surface cold core eddy in the Bay of Bengal during south-west monsoon season and explore the possibility to reconstruct the acoustic profile of the eddy by Stochastic Inverse method utilizing OAT's technique under peculiar characteristics viz, depth-limited and weak gradient environment. For the formulation of the Stochastic Inverse, both vertical and horizontal structure of the ocean has been modeled using empirical orthogonal modes.

Present OAT's simulation experiment results reveal that one can objectively map/monitor even the small mesoscale sub-surface cold core eddies by stochastic inverse technique. Keeping single source and receiver in the SOFAR channel separated probably by larger distances also under the above mentioned conditions in the Bay of Bengal.

Acknowledgement

Authors are thankful to Dr. S.R. Shetye, Director, NIO, Goa, and Dr. V.S.N. Murty, Scientist-in-charge, NIO, Regional Center, Visakhapatnam for their interest and encouragement. The OAT group of NIO, Goa during 1982-1997 was acknowledged for fruitful discussion. The authors would like to thank the reviewers for their valuable suggestions. This is NIO contribution number 4902.

Appendix-A

Ocean Model

Physical variability occurs in the ocean with space (scales of millimeters to planetary) and time (from seconds to geological times) due to external and internal forcing³³. Physical oceanographers are interested to study variability of ocean environment rather than its mean. Oceanic changes relevant to underwater acoustics are classified into mean and fluctuating components⁴³ with the following general model of the sound speed equation

$$C(r,t) = C_0(z) + \delta C(r) + \Delta C(r,t) \quad \dots (A1)$$

z – depth, t -time, r - three-dimensional position having characteristics: 1) a mean vertical profile $C_0(z)$ that represents local climatology ($C_0 \sim 1500$ m/s), 2) a mesoscale component $\delta C(r)$ (fronts, eddies etc) - deterministic with respect to the acoustic time scale ($\delta C/C_0 \sim 10^{-2}$), and 3) a statistical component $\Delta C(r,t)$ (i.e random with respect to the acoustic time scale, $\Delta C/C_0 \sim 10^{-4}$ that represents small scale fluctuations) caused by Internal Waves (IW), fine and microstructures. In the above equation the background profile is often taken as layered mean profile given by

$$C_0(z_k) = \frac{1}{n} \sum_{j=1}^n C_j^1(x_j, z_k) \quad \dots (A2)$$

Other choices can also be made, such as climatological mean or even a representative member of the vertical profiles.

Computational Procedures

Following Lawson and Hanson⁴⁴, 2D sound velocity perturbation $\delta C(x, z)$, (ignoring time dependency) is written as product of three matrices in component form:

$$\delta C(x, z) = \sum_{i=1}^r u_i(z)v_i(x)l_i^2 \quad \dots \text{ (A3)}$$

$x = 1, \dots, n; z = 1, \dots, m; r = \text{rank of } D$

where n is the number of vertical layers in the ocean model, m is the number of horizontal grid points, the $u_i(z)$ are the vertical modes and the $v_i(x)$ are the horizontal coefficients.

Eqn (B1) is expressed in Singular Value Decomposition (SVD) form:

$$D = U \Gamma V^T \quad \dots \text{ (A4)}$$

$(m \times n) (m \times r) (r \times r) (r \times n)$

The dimensions of matrices D , U , Γ and V^T are (m, n) , (m, r) , (r, r) , and (r, n) respectively. The matrices U and V are orthonormal i.e.; $U^T U = I_m$ and $V^T V = I_n$ where I_m and I_n are the identity matrices of order $(m \times m)$ and $(n \times n)$ respectively. In general, $U U^T \neq I_m$ and $V V^T \neq I_n$ and these matrices are called data and model resolution matrices. The matrix Γ is a diagonal matrix of nonzero ‘singular values’ of D in descending order $(l_1 > l_2 > \dots > l_r)$ and $r [r \leq \min(m, n)]$ is the rank of matrix D . Obviously, the rank of all the three component matrices will be r , and hence all diagonal elements of Γ are squares of singular nonzero values l_i^2 . U and V are the respective coupled eigen vector matrices for the eigenvalue problem defined as

$$(D D^T)u = l^2 u \quad \dots \text{ (A5)}$$

$$\text{and } (D^T D)v = l^2 v \quad \dots \text{ (A6)}$$

The matrices $D D^T$ and $D^T D$ are called the covariance matrices, of orders $(m \times m)$ and $(n \times n)$ respectively and, from which the EOF’s are generated. The two sets, i.e depth-dependent $s(z) = \{u_1, u_2, \dots, u_p\}$ and range-dependent $s(r) = \{v_1, v_2, \dots, v_p\}$ are the orthogonal vectors (column vectors of u and v) of the matrix D respectively and

$p(\leq r)$ are the number of factors to be considered. EOF depicts the underlying dynamics describe statistically to determine the direction of maximum variability. These directions called the ‘principal components’ of EOFs of the second order statistics or ‘moments’.

If $m < n$ then, first compute matrix U by solving eigen value problem (Eqn.B5) and matrix V is computed by relation $V = D^T U \Gamma^{-1}$.

If $m > n$ then, compute matrix V by solving eigen value problem (Eqn.B6) and matrix U is computed by relation $U = D V \Gamma^{-1}$.

Having computed the u_i , the modal amplitudes $a_i(x)$ at each horizontal grid points are easily computed by projecting the layered perturbation profiles on the layered EOF’s, i.e;

$$a_i(x) = \sum_{k=1}^r \delta C(x, z_k) u_i(z_k), i, k = 1, \dots, r \quad \dots \text{ (A7)}$$

where, i – indicates the mode index and n - the layer index. Here i can go to a number $p \leq r$ (rank of D), if we truncate the mode sum. This is done by judiciously selecting the p eigen vectors or ranking the singular values of the Γ matrix in descending order. We then spline fit the modes, their coefficients, and the mean profiles to get a field with continuous derivatives at any point. The mode contribution of sound velocity perturbation field in terms of percentage is as follows:

Closeness Ratio:

The ratio between the sum of the factors considered and that of data matrix (Kernel) is the measure of closeness of the model data³⁸:

$$\text{Measure of closeness} = \frac{\sum_{i=1}^p l_i^2}{\sum_{i=1}^r l_i^2} \quad \dots \text{ (A8)}$$

where r is the rank of the data matrix D (kernel) and $p \leq r$. The first eigen function, u_1 in depth dependent vector space $s(z)$, associated with the largest eigen value l_1^2 represents the gross features (i.e. $\|u_1^T D\|$) in the data in the least square sense, while the second function u_2 in the space $s(z)$ associated with second largest eigen value l_2^2 describes the residual mean square data [i.e. $\|u_2^T (D - (u_1 u_1^T D))\|$] in the least square sense and so on. The similar explanation can be given for range dependent vectors $s(r)$. The

closeness ratio is expressed in percentage to judge the contribution of different parameters.

$s(z)$ and $s(r)$ distribution of individual percentage contribution of j^{th} element of, k^{th} eigen function for present analysis are given by Ramana Murty *et.al.*⁴⁵

$$\left[\frac{u_{jk}}{\sum_{i=1}^m |u_{ik}|} \right] \left[\frac{l_k^2}{\sum_{i=1}^r l_i^2} \right] * 100 \quad \dots \text{ (A9)}$$

$$\left[\frac{v_{jk}}{\sum_{i=1}^n |v_{ik}|} \right] \left[\frac{l_k^2}{\sum_{i=1}^r l_i^2} \right] * 100 \quad \dots \text{ (A10)}$$

References

- 1 Mercer J.A. & Booker J.R., Long range propagation of sound through Oceanic mesoscale structures, *J.Geophys. Res*, 88, (1983) 689-700.
- 2 Robinson, A. R, *Eddies in marine sciences*, Springer Verlag, New York, (1983). Page ?
- 3 Prasanna Kumar S., Nuncio M., Jayu Narvekar, Ajay Kumar, Sardesai S., Desouza,S.N., Mangesh Gauns, Ramaiah N. & Madhupratap, M., Are eddies nature's trigger to enhance biological productivity in the Bay of Bengal?, *Geophys. Res. Lett.*, 31, (2004) L07309, doi: 10.1029/2003G1019274.
- 4 MODE group, Mid-ocean dynamics experiment, *Deep Sea Res*, 25, (1978) 859-910.
- 5 Richman, J.G., Wunsch C. & Hogg N.G., Space and time scales of mesoscale motion in the western North Atlantic, *Rev. Geophys. and Sp. Phys.*,15, 4, (1977) 385-420.
- 6 Chelton, D.B., DeSzoeke, R.A., Schlax, M.G., Naggar, K. E. & Siwertz, N., Geophysical variability of the first baroclinic Rossby radius of deformation, *J. Phys. Oceanogr.*, 28, (1998) 433-460.
- 7 Ram Sastry. A.A., & Balaramamurty, C., Thermal fields and oceanic circulation along the East coast of India, *Proc. of Indian Acad. of Sci.*, 46, (1957) 293-323.
- 8 Rao, D.P. & Sastry, J.S., Circulation and distribution of some hydrographical properties during the late winter in the Bay of Bengal, *Mahasagar-Bull. Natl.Inst. Oceanogr.*, 14, (1981) 1-16.
- 9 Legeckis, R., Satellite observations of a western boundary current in the Bay of Bengal *J.Geophys. Res.*, 92, (1987) 12974-12978.
- 10 Babu, M.T., Prasanna Kumar S. & Rao D.P., A subsurface cyclonic eddy in the Bay of Bengal. *J. Mar. Res.*, 49, (1991) 403-410.
- 11 Babu M.T. Sarma, Y.V.B., Murty, V.S.N. & Vethamony, P., On the circulation in the Bay of Bengal during northern spring inter-monsoon (March-April) 1987 *Deep sea Res. II* 50, (2003) 855-865.
- 12 Madhusoodhanan, P. & James, V.V., Thermohaline features of the subsurface cyclonic eddy in the south central Bay of Bengal during August 1999, *Proc. Ind. Acad. Sci (Earth and Planet Sci.)*, 112, (2003) 233-237.
- 13 Swallow J.C., *Eddies in the Indian Ocean* (Ed. By A.R.Robinson), Springer_Verlag Berlin Heidelberg, (1983).
- 14 Prasanna Kumar S., Babu M.T. & Rao D.P., Energy and generating mechanism of a subsurface, cold eddy in the Bay of Bengal, *Indian J. Mar. Sci.*, 21, (1992) 140-142.
- 15 Munk, W.H. & Williams, G.O., Acoustic Oceanography, *Nature*, 267, (1977) 774-778.
- 16 Falkowski, P.G., Ziemann, D., Kolber, Z. & Bienfang, P.B., Role of eddy pumping in enhancing primary production in the Ocean, *Nature*, 352, (1991) 55-58.
- 17 McGillicuddy, D.J., Robinson, A.R., Siegel, D.A., Jannasch, H.W., Johnson, R., Dickey, T.D., McNeil, J., Michaels, A.F. & Knap, A.H., Influence of mesoscale eddies on new production in the Sargasso sea, *Nature*, 394, (1998) 263-266.
- 18 Oschlies, A. & Garcon, V. Eddy-induced enhancement of primary production in a model of the North Atlantic Ocean, *Nature*, 394, (1998) 266-269.
- 19 Abraham, E.R., Law, C.S., Boyd, P.W., Lavender, S.J., Maldonado, M.T. & Bowie, A.R. Importance of stirring in the development of an iron-fertilized phytoplankton bloom, *Nature*, 407, (2000) 727-730.
- 20 Ali M.M, Rashmi Sharma & Robert Cheney, *An Atlas of the North Indian Ocean Eddies From TOPEX Altimeter Derived Sea Surface Heights*, Indian Space Research Organisation, Bangalore, India (ISRO)-SAC-SP-69-98, August, (1998).
- 21 Munk, W.H & Wunsch, C, Ocean acoustic Tomography: A scheme for large scale monitoring, *Deep Sea Res.*, 26, (1979) 123-161.
- 22 Cornuelle, B.D., Inverse methods and results from the 1981 ocean acoustic tomography experiment, *Ph.D. Thesis*, Woods Hole Oceanographic Institution, Mass.(1983).
- 23 Radon, J., Uber die bestimmung von funktionen durch ihre integralwerte langs gewisser mannigfaltigkeiten, *Ber Saechs, Akademie der Wissenschaften, Leipzig, Mathematisch-Physikalische Klasse*, 69,(1917) 262-277.
- 24 Park, J.H., *Study on the analyses of the Coastal Acoustic Tomography Data*, Doctor Dissertation, Graduate School of Engineering, Hiroshima University, (2001).
- 25 Liebelt, P.B., *An Introduction to Optimal Estimation*, Addison-Wesley Publishing Company, London, (1967) 272.
- 26 Menke W., *Geophysical data analysis: Discrete Inverse Theory*, Academic Press, San Diego, (1989).
- 27 Aki. K. & Richards, P.G., *Quantitative Seismology, theory and methods*, W.H. Freeman, San Francisco, (1980).
- 28 Prasanna Kumar, S., Ramana Murty, T.V., Somayajulu, Y.K., Saran, A.K. Navelkar, G.S., Almeida, A.M., Fernando, V. & Murty, C.S., Acoustic Tomography Experiment in the Eastern Arabian Sea, *ACUS. Act. Acus.t.* 85, (1999) 31-38.
- 29 Hamilton, K.G., Siegmann, W.L., & Jacobson, M.J., Simplified calculation of ray phase perturbations due to ocean environmental variations *J. Acoust. Soc. Am.*, 67, (1980) 1193-1206.
- 30 Pedlosky, J., *Geophysical Fluid Dynamics*, Springer-Verlag, New York, (1980) 625.
- 31 Chen, C.T. & Millero, F.J., Speed of sound in sea water at higher pressure, *J. Acoust Soc. America*, 60, (1977) 129-135.

- 32 Denman, K.L. & Dower, J.F., *Patch dynamics, in Encyclopedia of Ocean Sciences*, edited by J.H. Steele, et al., Academic Press, New York, (2001) 2107-2114.
- 33 Robinson, A.R. & Ding Lee, *Oceanography and Acoustics*, AIP Press, (1994) 257.
- 34 Wiggins, R.A., The general linear inverse problem: Implication of surface waves and free oscillations for earth structure, *Rev. Geophys.*, 10, (1972) 251-285.
- 35 Stidd, C.K., The use of eigen vectors for climate estimates, *J. Appl Meteor.*, 6, (1967) 255-271.
- 36 Winant, C.D., Inman, D.L. & Nordstorm, C.E., Description of seasonal beach changes using empirical eigen functions, *J. Geophys. Res.*, 80, (1975) 1979-1986.
- 37 Aubray, D., *Statistical and dynamical prediction of changes in natural sand beaches*, Ph.D.dissertation, Scripps Institute of Oceanography, San Diego, California (1978).
- 38 Ramana Murty, T.V., Veerayya, M. & Murty, C.S., Sediment size distribution of the beach and near shore environs along central west coast of India: An analysis using EOF, *J. Geophys. Res.*, 91, (1986) 8523-8536.
- 39 Fukumori, I., *Efficient representation of the hydrographic structure of the North Atlantic Ocean and aspects of the circulation from objective methods*, Ph.D. dissertation (Joint program in Oceanography, Massachusetts Institute of Technology – Woods Hole Oceanographic Institution), (1989) 236.
- 40 Prasanna kumar, S., Ramana Murty, T.V, Somayajulu, Y.K., Chodankar, P.V. & Murty, C.S., Reference sound speed profile and Related Ray Acoustics of Bay of Bengal for Tomographic Studies, *Acustica*, 80, (1994) 127-137.
- 41 Jackson, D.D., Interpretation of inaccurate, insufficient and inconsistent data, *Geophys. J.Astron.Soc.*, 28, (1972) 97-109.
- 42 Ramana Murty, T.V., Somayajulu, Y.K., Mahadevan, R., Murty C.S., & Sastry, J.S., A solution to the inverse problem in Ocean acoustics, *Defence Science Journal*, 42, 2, (1992) 89-101.
- 43 DeSanto, J.A., Theoretical Methods in Ocean Acoustics, *In Ocean Acoustics*, edited by DeSanto J.A., (1979) 7-77.
- 44 Lawson C.L. & Hanson R.J. *Solving least squares problem*, Prentice Hall, New Jersey, (1974).
- 45 Ramana Murty, T.V., Mohan Rao, K., Malleswara Rao, M.M., Lakshmi Narayana, S. & Murty, K.S.R., Sediment – size distribution of innershelf off Gopalpur, Orissa Coast using EOF analysis, *J. Geolo. Soc. India*, 69, (2007) 133-138.